


Stochastic Channel Modeling for Railway Tunnel Scenarios at 25 GHz

Danping He , Bo Ai, Ke Guan, Zhangdui Zhong,
Bing Hui, Junhyeong Kim, Heesang Chung, and Ilgyu Kim

More people prefer using rail traffic for travel or for commuting owing to its convenience and flexibility. The railway scenario has become an important communication scenario in the fifth generation era. The communication system should be designed to support high-data-rate demands with seamless connectivity at a high mobility. In this paper, the channel characteristics are studied and modeled for the railway tunnel scenario with straight and curved route shapes. On the basis of measurements using the “Mobile Hotspot Network” system, a three-dimensional ray tracer (RT) is calibrated and validated for the target scenarios. More channel characteristics are explored via RT simulations at 25.25 GHz with a 500-MHz bandwidth. The key channel parameters are extracted, provided, and incorporated into a 3rd-Generation-Partnership-Project-like stochastic channel generator. The necessary channel information can be practically realized, which can support the link-level

and system-level design of the communication system in similar scenarios.

Keywords: MHN, Millimeter wave channel, Railway communication, Ray tracing simulation, Stochastic channel modeling.

I. Introduction

Currently, a growing number of people prefer to take rail traffic for traveling and commuting because of the comfortable experience and convenience that it provides. In order to meet the goals of efficiency, safety, and convenience, rail traffic is expected to be “smart” in the fifth generation (5G) era. The railway infrastructure, trains, travelers, and goods will be increasingly interconnected. Thus, rail-traffic communication has become an increasingly important topic, and seamless high-data-rate wireless connectivity is desired. Consequently, railway communications are required to evolve from handling only the critical signaling applications to support various high-data-rate applications [1], [2]. In order to realize this vision, the millimeter wave (mmWave) band has become important to overcome spectrum scarcity, and many efforts have been carried out to develop novel technologies such as multiple-input–multiple-output (MIMO) beamforming [3]–[6], resource allocation, and multiple access. The 5GCHAMPION project [7], funded by the H2020 Europe–Korea collaborative program, aims to develop key enabling technologies for a proof-of-concept environment to be showcased at the 2018 Winter Olympics in PyeongChang, Korea. One of the key applications is to provide a high-mobility broadband connection via a 5G mmWave high-capacity backhaul in the range of 24 GHz to 28 GHz. The

Manuscript received Sept. 15, 2017; revised Nov. 21, 2017; accepted Nov. 30, 2017.

Danping He (hedanping@bjtu.edu.cn), Bo Ai (boai@bjtu.edu.cn), Ke Guan (corresponding author, kguan@bjtu.edu.cn), and Zhangdui Zhong (zhdzhong@bjtu.edu.cn) are with the State Key Laboratory of Rail Traffic Control and Safety, Beijing Jiaotong University and also with the Beijing Engineering Research Center of High-speed Railway Broadband Mobile Communications, China.

Bing Hui (huibing@etri.re.kr), Heesang Chung (hschung@etri.re.kr), and Ilgyu Kim (igkim@etri.re.kr) are with the 5G Giga Service Research Laboratory, ETRI, Daejeon, Rep. of Korea.

Junhyeong Kim (jhkim41jf@kaist.ac.kr) is with the 5G Giga Service Research Laboratory, ETRI, Daejeon, Rep. of Korea and the School of Electrical Engineering, Korea Advanced Institute of Science and Technology, Daejeon, Rep. of Korea.

This is an Open Access article distributed under the term of Korea Open Government License (KOGL) Type 4: Source Indication + Commercial Use Prohibition + Change Prohibition (<http://www.kogil.or.kr/info/licenseTypeEn.do>).

Electronics and Telecommunication Research Institute (ETRI), as a member of the 5GCHAMPION project, prototyped a new wireless communication system named “Mobile Hotspot Network (MHN),” which works in the range of 24 GHz to 30 GHz with 125-MHz, 250-MHz, 500-MHz, and 1-GHz bandwidths. It targets the support of services with a data rate of gigabits per second with a speed over 400 km/h [8], and several trials have been carried out in the Seoul Subway.

Standardization organizations are becoming active in the promotion of the priority in standardizing mmWave high-speed railway (HSR) communication technologies as well. In IEEE 802.15, the “High Rate Rail Communications” interest group was founded in 2014 to invite proposals and studies on broadband HSR communications. In 2016, the Macro + Relay deployment for the HSR scenario was agreed to be included in the 3rd Generation Partnership Project (3GPP) evaluation [9]–[11]. The working frequency is around 30 GHz, and the bandwidth is above 100 MHz. Each baseband unit is attached to three remote radio heads (RRHs). RRHs are uniformly deployed along the two rail tracks. The suggested distance from the RRH to the rail track is 5 m. MIMO systems with a unidirectional beam or bidirectional beam are recommended to compensate the high attenuation of mmWave band propagation. A correct understanding of the mmWave propagation channel characteristics in railway scenarios is mandatory to effectively support the design and evaluation of communication systems [12]. However, the mmWave band channel has been explored mainly for urban indoor and outdoor scenarios [13]–[16]. According to [17], the railway environments are divided into 19 scenarios on the basis of a review of four different HSR lines and eight HSR stations. Five applications are defined in [1], [2] from the viewpoint of propagation and wireless channels, including the train-to-infrastructure, intercar, intracar, inside-the-station, and infrastructure-to-infrastructure communications. The route shapes are also very important to the mobility and communication design. Straight and curved route shapes are typical in railways. However, most of the current studies focus on the straight route owing to a lack of measurements of the curved route. The works on existing standardized channel modeling rarely provide dedicated parameters for railway scenarios [18], [19].

In this study, the channel characteristics of tunnel scenarios are studied and modeled. Measurements are conducted in the 5G mmWave band in Seoul Subway Line 8 for both straight and curved routes. The 3D environments of the measurement campaign are modeled, and a ray tracer (RT) is calibrated and leveraged with the measurements to

explore more channel characteristics. The key time-variant channel parameters and their correlations are modeled. The stochastic channels are realized on the basis of a 3GPP-like channel generator. The validated results indicated that the 3GPP-like framework is suitable for describing high-mobility scenarios. With the provided parameters, researchers and engineers can practically realize 3GPP-like channels to evaluate the designed communication technology in similar scenarios.

The remainder of this paper is organized as follows: The measurements and RT calibration are introduced in Section II. The channel parameters are analyzed and modeled in Section III. The conclusions are drawn in Section IV.

II. Measurement Campaign and Ray-Tracer Calibration

1. Measurement Campaign

An MHN Radio Unit (mRU), which is also called a transmitter (Tx) in this work, is installed on the side wall of the tunnel (see Fig. 1(a)), and the MHN Terminal Equipment (mTE), which is also called a receiver (Rx), is installed at the middle of the front window in the cab. The heights of the mRUs and mTE are 3.2 m and 3.0 m, respectively. The shortest two-dimensional distance between an mRU and the mTE is 2.8 m. The antenna used for both the mRUs and mTE is an 8×8 patch array antenna, as shown in Fig. 1(b). The measurements are conducted by installing the MHN test bed in Seoul Subway Line 8 from Jamsil station to a place after Songpa station, as shown in Fig. 1(c). A curved route is connected to a straight route in the measurement campaign. The radius of curvature of the tunnel is around 500 m. The lengths of the curved route and the straight route are 600 m and around 1,700 m, respectively. The half-power beam width (HPBW) is 8° , and the antenna gain is 22 dBi with vertical–horizontal dual polarization, as shown in Fig. 2. The main lobes of both the mRUs and mTE are pointed at each other, and handover occurs when the train is near an mRU. Three mRUs (mRU1, mRU2, and mRU3) are installed in the curved route with distances less than 300 m to guarantee a stable communication link under possible non-line-of-sight conditions. Only two mRUs (mRU4 and mRU5) are installed on the straight route, and the largest tested link distance is 1,180 m at mRU5.

2. Environmental Modeling

As shown in Fig. 3, the cross section of the tunnel is a rectangle with pylons in the middle that separate the

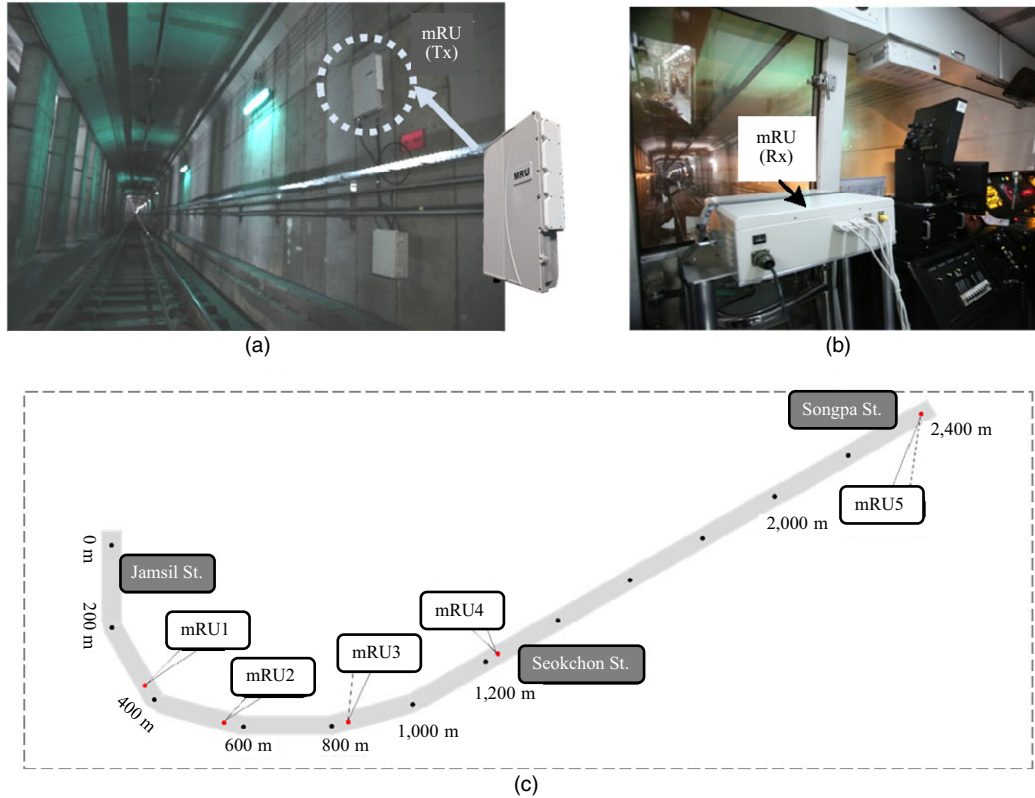


Fig. 1. Measurement campaign: (a) MHN test bed mRU (Tx) installation details, (b) MHN test bed mRU (Rx) installation details, and (c) measurement along Seoul Subway Line 8.

two-way tracks. The width of the tunnel is 13.7 m, and the height is 7.1 m. Figure 4 shows the constructed straight and curved tunnel models for the RT simulation. The side wall and pylons are made of concrete, the tracks are made of metal, and the train is made of metal (train body) and glass (windows). The lengths of the two models are greater than 1,200 m, which are longer than the measured length.

3. Ray-Tracer Calibration

The deployment and configuration of the mRUs and mTE in the RT are the same as those in the measurement campaign. A calibration algorithm based on a simulated annealing method [21], [22] is employed to reduce the error by seeking the appropriate material parameters. The calibrated dielectric parameters and scattering coefficients of the directive scattering model [23] of concrete, glass, and metal are provided in Table 1; note that the calibrated transmission loss of glass is 833.33 dB/m (the equivalent attenuation with a thickness of 6 mm is 5.0 dB). Figure 5 shows the progress of the calibration. As the number of iterations increases, the calibration error decreases and

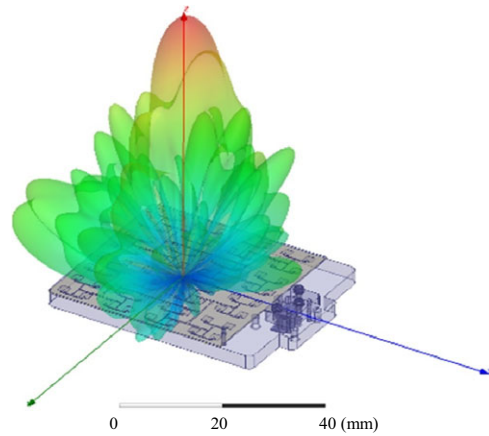


Fig. 2. Antenna pattern of mRU and mTE (V-polarization): HPBW = 8°, Gain = 22 dBi.

saturates after the 4th iteration. The received power of snapshot s is expressed as $P_{rx}(s) = \sum_{\tau=0}^{\tau_{max}} |h(s, \tau)|^2$, and Fig. 6 compares the cumulative distribution functions (CDFs) of the error of P_{rx} (mW) before and after RT calibration. The mean absolute errors of the calibrated RT are 4.2×10^{-5} mW (straight route) and 5.1×10^{-5} mW

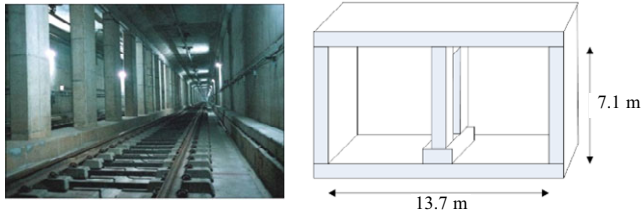


Fig. 3. Cross section of Seoul Subway Line 8 [20].

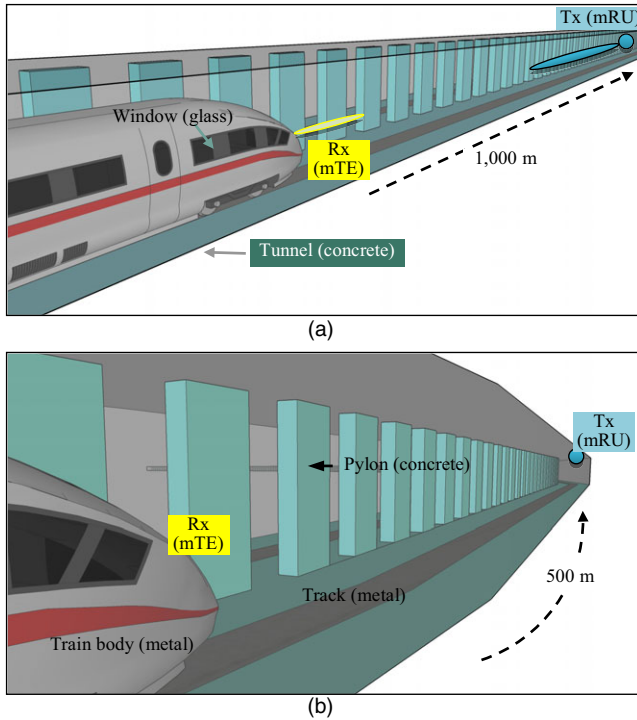


Fig. 4. (a) Straight and (b) curved tunnel scenarios.

Table 1. Material parameters.

Material name	ϵ'_r	ϵ''_r	A (dB/m)	S	α
Concrete	5.310	0.307	Not involved	0.0011	40
Glass	6.270	0.149	833.33	6.27×10^{-4}	91
Metal	1.000	10^7	INF	0	0

(curved route); the standard deviation (STD) of the absolute errors in milliwatts are 6.3×10^{-5} and 7.6×10^{-5} , respectively. Thus, the calibrated RT results match the measurements well. Thereafter, intensive reliable RT simulations are conducted to practically explore more characteristics (azimuth/elevation angular spreads, omnidirectional channel characteristics) that could not be captured in the measurements. Figure 7

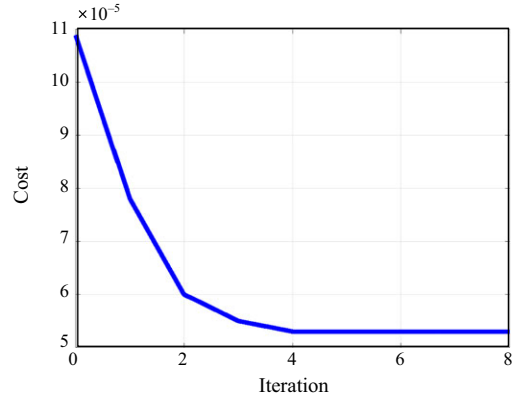


Fig. 5. Progress of the calibration results.

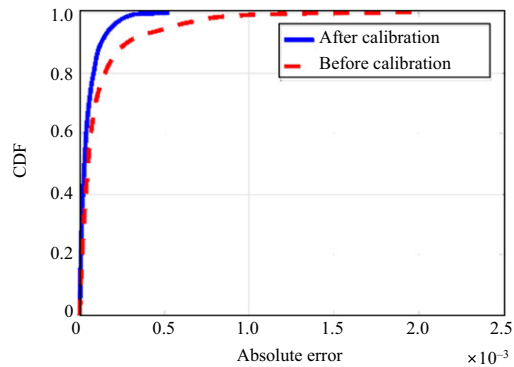


Fig. 6. CDF of the absolute errors before and after calibration.

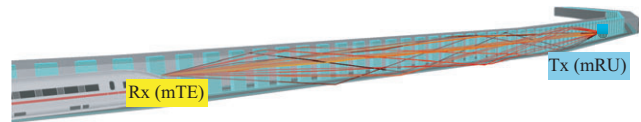


Fig. 7. Rays traced for the straight and curved tunnels.

shows the transmitted and reflected rays traced for the curved tunnel.

III. Simulation and Analysis of the Results

The MHN system works from 24 GHz to 30 GHz and supports a maximum bandwidth of 1 GHz. Recently, the Korean government released a regulation that the total effective isotropic radiated power should be smaller than 36 dBm, and the allocated frequency is 25 GHz to 25.5 GHz, which is lower than that in the measurements. To re-evaluate the system performance, accurate channels are needed for straight and curved routes with new parameters. RT simulations are conducted at 25.25 GHz with omnidirectional antennas at the Tx and Rx. As most

services have high requirements for the downlink in practice, the channel propagation and characteristics are analyzed by considering an mRU as the Tx and the mTE as the Rx in this work. The travel distance of the Rx is 1,000 m for the straight route and 350 m for the curved route. The distance between the Tx and the track center is 2.8 m. The snapshot sampling interval is 0.1 m. Thus, the total numbers of snapshots are 10,001 for the straight-route scenarios and 5,001 for the curved-route scenarios. Up to the 10th order of reflection, scattering and transmission are considered in the simulation.

1. Path-Loss Model

Figure 8 shows how the path loss PL varies with the Tx–Rx distance d . The “A-B” model is employed in this work to fit the PL :

$$PL = A \log_{10}(d) + B + X_{\sigma}, \quad (1)$$

where d is the distance between the Tx and the Rx, A is the slope, B is the intercept, and X_{σ} is the shadow fading (SF), which can be expressed as a zero-mean Gaussian random variable with an STD of σ . The fitting results are compared in Fig. 8 as well. As can be seen, a breakpoint at a distance d_{bp} exists in both scenarios. When $d \leq d_{bp}$, the region is defined as a near region. On the contrary, the far region is where $d > d_{bp}$. The extracted parameters are provided in Table 2. d_{bp} of the straight tunnel is five times that of the curved tunnel. In both scenarios, A_{near} is less than A_{far} . It is noteworthy that the train body, which is made of metal, blocks the direct transmission path at the very beginning of the near region. Thus, only the reflected and scattered rays can reach the Rx, which results a great difference between the simulated path loss and the free-space path loss. In the far region, the path loss in the curved tunnel is more severe than that in the straight tunnel, and A_{curved} is more than two times $A_{straight}$. σ_{curved} is smaller than $\sigma_{straight}$ in both the near and far regions. The correlated distance of SF is defined as λ_{SF} , and the units are meters. λ_{SF} of the near region is smaller than that

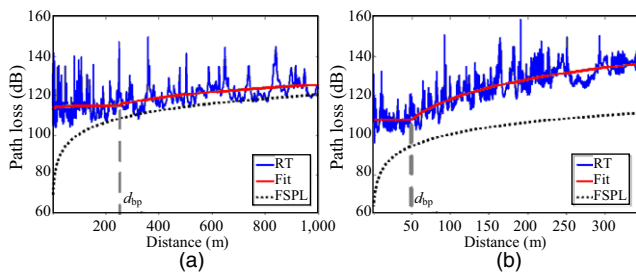


Fig. 8. Path losses of both scenarios: (a) path loss of the straight tunnel and (b) path loss of the curved tunnel.

Table 2. Extracted parameters for the PL .

PL	Straight tunnel ($d_{bp} = 257.2$ m)		Curved tunnel ($d_{bp} = 50$ m)	
	Near	Far	Near	Far
A	0.64	16.50	0	33.40
B	113.56	76.06	107.76	51.45
σ (dB)	5.93	4.96	4.53	4.83
λ_{SF} (m)	1.10	1.70	1.00	1.10

of the far region, and λ_{SF} of the curved tunnel is at least four times shorter than that of the straight tunnel. This observation indicates that the variation in the straight tunnel is less than that of the curved tunnel.

2. Delay Spread and Rician K-Factor

Figure 9 shows the CDFs of the root-mean-square (RMS) delay spreads (DSs) σ_{τ} of both scenarios. σ_{τ} can be fitted by a lognormal distribution function (Table 3). In the straight tunnel, the mean RMS delay spread in the near region is larger than in the far region. In the curved tunnel, the values of σ_{τ} for the near region and far region are similar and are fitted with the same model. The mean value and the range of variation of the straight tunnel are smaller than those of the curved tunnel. A Rician distribution indicates the presence of a specular dominant component in the channel over other very weak paths, and its probability density function (PDF) is expressed as

$$Px(x) = \frac{x}{\sigma_n^2} e^{-\frac{x^2 + A^2}{2\sigma_n^2}} I_0\left(\frac{Ax}{\sigma_n^2}\right), \quad (2)$$

$$K = 10 \log_{10}\left(\frac{A^2}{2\sigma_n^2}\right), \quad (3)$$

where I_0 is the modified Bessel function of the first kind and zeroth order, A is the amplitude of the

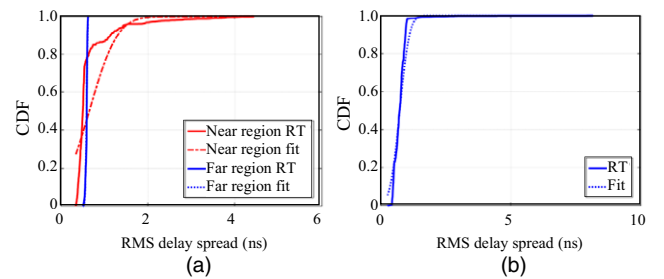


Fig. 9. Delay spreads of both scenarios: (a) DS of the straight tunnel and (b) DS of the curved tunnel.

Table 3. Extracted parameters for the DS.

DS	Straight tunnel		Curved tunnel
	Near	Far	
Mean log10 (ns)	-9.19	-9.24	-9.14
σ_{DS} log10 (ns)	-9.29	-10.67	-9.53
λ_{DS} (m)	6.80	20.30	4.60
r_{DS} (m)	2.83	2.83	2.57

dominant path, and σ_n is the STD of all other weak path amplitudes. The amplitudes are computed by using the peak values of the channel impulse responses. The Rician K-factor (KF) is expressed by (3). The CDFs are compared in Fig. 10, and the fitting results are summarized in Table 4. The mean KFs of both scenarios are greater than 24 dB. In the far region of the straight tunnel, the mean value is greater than that in the near region. The mean KF of the curved-tunnel scenario is the lowest, indicating that multipath components contribute more significantly compared to the straight tunnel. The correlated distance λ_{KF} of the curved tunnel is much less than that of the straight tunnel.

3. Angular Domain

According to the 3GPP definition [24], the conventional angular spread (AS) calculation for the composite signal is given by

$$\sigma_{AS} = \sqrt{\frac{\sum_{n=1}^N \sum_{m=1}^M (\theta_{n,m,\mu})^2 \cdot P_{n,m}}{\sum_{n=1}^N \sum_{m=1}^M P_{n,m}}},$$

where $P_{n,m}$ is the power for the m th subpath of the n th path, $\theta_{n,m,\mu}$ is defined as

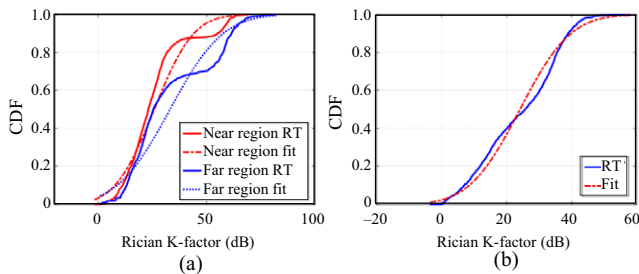


Fig. 10. Rician K-factors: (a) KF of the straight tunnel and (b) KF of the curved tunnel.

Table 4. Extracted parameters for the KF.

KF	Straight tunnel		Curved tunnel
	Near	Far	
Mean (dB)	25.70	32.95	24.02
σ_{KF} (dB)	14.23	19.15	12.24
λ_{KF} (m)	11.20	14.60	2.10

$$\theta_{n,m,\mu} = \begin{cases} 2\pi + (\theta_{n,m} - \mu_\theta) & \text{if } (\theta_{n,m} - \mu_\theta) < -\pi \\ (\theta_{n,m} - \mu_\theta) & \text{if } |\theta_{n,m} - \mu_\theta| \leq \pi \\ 2\pi - (\theta_{n,m} - \mu_\theta) & \text{if } (\theta_{n,m} - \mu_\theta) > \pi \end{cases},$$

μ_θ is defined as

$$\mu_\theta = \frac{\sum_{n=1}^N \sum_{m=1}^M \theta_{n,m} \cdot P_{n,m}}{\sum_{n=1}^N \sum_{m=1}^M P_{n,m}},$$

and $\theta_{n,m}$ is the angle of arrival/departure of the m th subpath of the n th path. m is 1 for RT simulation results.

The RMS ASs of both scenarios are shown in Fig. 11. The fitting parameters are listed in Table 5. ASA, ASD, ESA, and ESD are the angular spreads of the azimuth angle of arrival (AoA), the azimuth angle of departure, the elevation angle of arrival (EoA), and the elevation angle of departure, respectively. The ASs of the straight tunnel in the far region are the smallest with the smallest variation. λ_{AS} of the far region of the straight route is the largest compared to the others (Table 6).

4. Cross-Correlation between the Key Parameters

The cross-correlations are computed for the aforementioned parameters. Tables 7 and 8 summarize the parameters for the near and far regions of the

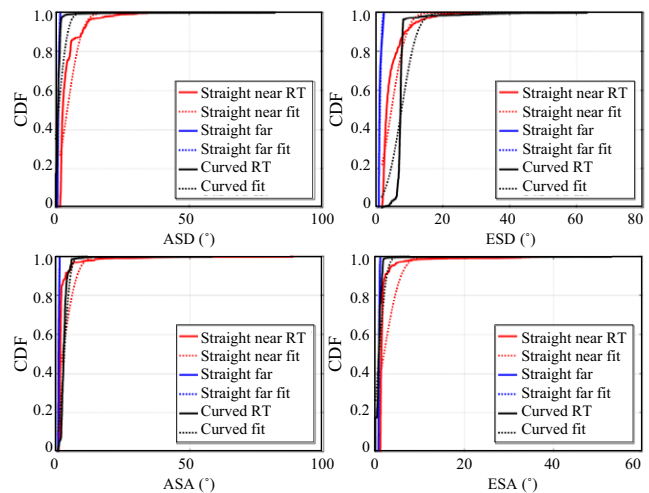


Fig. 11. CDFs of the ASs.

Table 5. Extracted parameters for the ASs.

ASD	Straight tunnel		Curved tunnel
	Near	Far	
Mean log10 (°)	0.63	9.65×10^{-4}	0.02
σ_{ASD} log10 (°)	0.64	-0.52	0.44
λ_{ASD} (m)	6.00	19.40	2.90

ESD	Straight tunnel		Curved tunnel
	Near	Far	
Mean log10 (°)	0.65	0.03	0.87
σ_{ESD} log10 (°)	0.56	-0.38	0.57
λ_{ESD} (m)	2.90	17.50	4.80

ASA	Straight tunnel		Curved tunnel
	Near	Far	
Mean log10 (°)	0.37	-0.04	0.47
σ_{ASA} log10 (°)	0.62	-0.76	0.26
λ_{ASA} (m)	6.95	19.90	4.00

ESA	Straight tunnel		Curved tunnel
	Near	Far	
Mean log10 (°)	0.28	-0.07	-0.07
σ_{ESA} log10 (°)	0.47	-0.94	0.12
λ_{ESA} (m)	15.45	20.00	4.20

straight tunnel, respectively. The cross-correlation of the DS and SF is positive in both regions, whereas the correlation between the DS/SF and other parameters are negative. Further, the cross-correlations of the other parameters significantly increase in the far region. When the diversity of multipath components (MPCs) increases, the variation in the SF increases as well. When the DS increases/decreases, the multipath components are more/less diverse in the time domain. The DS and SF are positively correlated, indicating that the SF is likely to vary with a similar trend as the DS. However, the angles are constrained within the narrow propagation region, and the range of ASs in the far region is less than that in the near region of the straight tunnel. Thus, the variations in the delays of rays barely influence the angles, especially in the far region of the straight tunnel. In the curved tunnel (see Table 8), the KF and SF are barely correlated with the other parameters. In both scenarios, the ASs are strongly correlated.

5. Polarization

The cross-polarization ratio (XPR) refers to the field received in the vertical (horizontal) copolarization relative

Table 6. Cross-correlation of the straight tunnel in the near region.

	DS	KF	SF	ASD	ASA	ESD	ESA
DS	1	0.52	0.20	0.87	0.76	0.83	0.78
KF		1	-0.12	0.65	0.23	0.64	0.21
SF			1	0.13	0.18	0.08	0.17
ASD				1	0.59	0.76	0.57
ASA					1	0.53	0.92
ESD						1	0.61
ESA							1

Table 7. Cross-correlation of the straight tunnel in the far region.

	DS	KF	SF	ASD	ASA	ESD	ESA
DS	1	-0.65	0.11	-0.75	-0.68	-0.72	-0.64
KF		1	0.01	0.96	0.98	0.89	0.99
SF			1	-0.01	-0.01	-0.03	0.01
ASD				1	0.97	0.94	0.96
ASA					1	0.94	0.99
ESD						1	0.89
ESA							1

Table 8. Cross-correlation of the curved tunnel.

	DS	KF	SF	ASD	ASA	ESD	ESA
DS	1	0.12	0	0.45	0.84	0.69	0.57
KF		1	-0.03	0.07	-0.17	0.05	0.01
SF			1	0.03	-0.03	0.02	0.07
ASD				1	0.47	0.52	0.67
ASA					1	0.60	0.69
ESD						1	0.47
ESA							1

to the field transmitted in the vertical polarization (horizontal) and received horizontal polarization (vertical). The XPR is expressed as

$$XPR = 20\log_{10}\left(\frac{E_{co}}{E_{cross}}\right).$$

The XPRs are fitted as a normal distribution (Fig. 12), and Table 9 summarizes the parameters. The smallest XPRs are negative in both scenarios with a probability of less than 20%, indicating that the copolarization configuration outperforms the cross-polarization configuration with a very large chance. The depolarization is the most severe in the

far region of the straight tunnel, as the mean XPR and minimum XPR are the smallest compared with the others. Thus, a dual polarization configuration at the Tx and Rx is suggested.

6. Clustering

The clustering procedure is realized by using a K-power-means algorithm clustering algorithm by considering the power, delay, AoA, and EoA. Twenty clusters are generated for both scenarios. The per-cluster parameters are summarized in Table 10. The per-cluster parameters in the far region of the straight tunnel are the smallest compared to the others.

7. Validation of the Channel Models

With all of the provided parameters in this work, stochastic channels can be generated by using a 3GPP-like channel generator. The QuaDRiGa channel generator [25], which includes all of the features of the 3GPP channel framework and supports the evolution of time-variant channel parameters, is used to realize and validate the channels. The deployment configuration and mobility patterns of the Tx and Rx are exactly the same as those in the RT, as shown in Fig. 13. Two segments

are defined on the basis of the different values of d_{bp} of the two scenarios. Examples of the values of PL of the generated channels are shown in Fig. 14. By running QuaDRiGa 10^5 times, the mean absolute error of PL is 2.5 dB, and the error in the PL coefficient is 0. The corresponding examples of the DS and KF are shown in Fig. 15. The mean absolute errors of the means and STDs are also 0. The validated parameters and the channel generator maintain consistency in the distribution of the large-scale parameters. As a result, the results of this work can be used to practically evaluate link/system-level technologies for similar tunnel scenarios.

IV. Conclusion

In this study, the channel characteristics are analyzed and modeled for railway tunnel scenarios in the mmWave band. Straight and curved route shapes are defined, and the 3D environment models are available online for free to download. Measurements are conducted inside the tunnel of a Seoul subway line. A 3D ray tracer is calibrated to ensure that the environment model and material parameters are practically close to reality. The transmission loss of the front window is 5 dB, and the dielectric parameters of the considered materials are obtained. The path loss, RMS delay spread, Rician K-

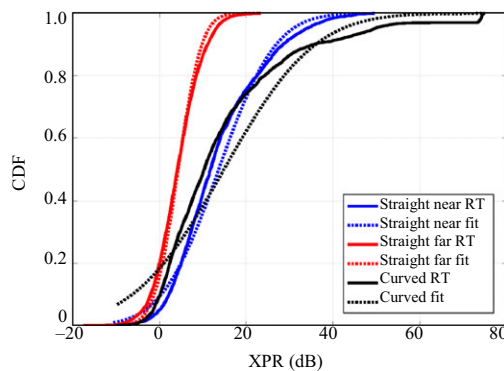


Fig. 12. Comparison of the XPRs.

Table 9. Extracted parameters for the XPR.

XPR	Straight tunnel		Curved tunnel
	Near	Far	
Mean (dB)	13.65	4.29	14.86
σ_{DS} (dB)	10.31	5.14	16.45

Table 10. Per-cluster parameters.

	Straight tunnel		Curved tunnel
	Near	Far	
SF (dB)	3	3.0	1.0
ASD (°)	2	0.5	0.5
ESD (°)	3	0.4	4.0
ASA (°)	1	0.4	2.0
ESA (°)	1	0.4	0.4

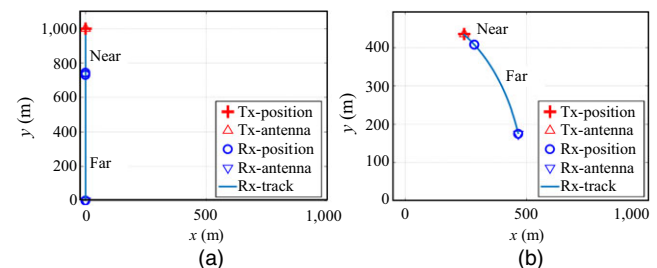


Fig. 13. Generated mobility patterns for both scenarios: (a) straight tunnel layout and (b) curved tunnel layout.

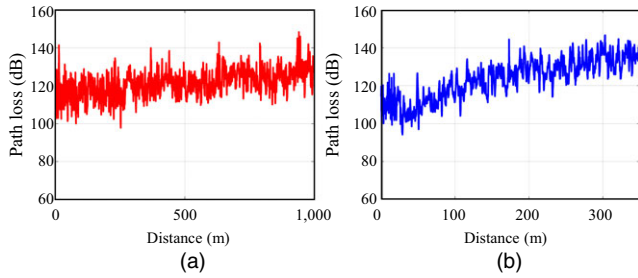


Fig. 14. Generated values of PL using the extracted parameters: (a) PL of the straight tunnel and (b) PL of the curved tunnel.

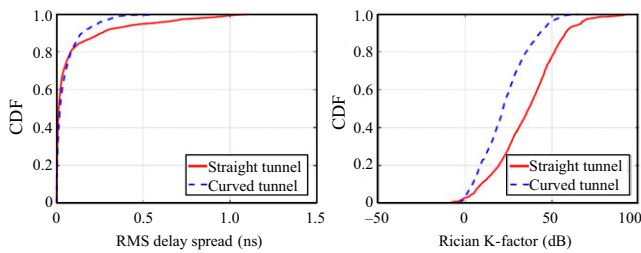


Fig. 15. Generated RMS delay spread and Rician K-factors for both scenarios using the extracted parameters.

factor, 3D angular spreads, and polarizations are extracted from the calibrated RT simulation, and the distributions and correlations are modeled. On the basis of a 3GPP-like channel modeling framework and the QuaDRiGa channel generator, the provided parameters are validated. The work of this paper indicates that the RT simulator can be integrated with channel measurements to analyze more channel characteristics. Moreover, the 3GPP-like framework and QuaDRiGa generator are suitable for describing high-mobility scenarios. With the provided parameters in this work, researchers and engineers can practically realize channels to evaluate the designed communication technology in similar scenarios. Moreover, the main observations from this work are summarized as follows:

- A break point exists in both scenarios, and d_{bp} of the straight tunnel is larger than that of the curved tunnel. Thus, two sets of parameters should be extracted, and special attention should be paid when implementing a stochastic channel generator.
- The correlated distances of the key parameters in the far region are larger than those in the near region, meaning that the channel characteristics vary more drastically in the near region.
- Owing to the drastic variation in the multipath components, the PL slopes in the near region of both scenarios are approximately 0, which makes PL barely

vary with the distance. In the far region, the curved tunnel suffers more path loss than that in the straight tunnel.

- The DS and SF are less correlated with the other parameters in the far region of the straight tunnel, whereas the other parameters are more correlated with each other. In the curved tunnel, the KF and SF are barely correlated with the other parameters. The ASs are strongly correlated in both scenarios.
- The copolarization configuration outperforms the cross-polarization configuration with more than 80% probability. The depolarization in the far region of the straight tunnel is the most severe compared to those of the others. Thus, a dual polarization configuration at the Tx and Rx is suggested.

In future work, different Tx/Rx configurations and multilink channel simulations will be explored. The influence of different configurations on link-level and system-level technologies will be evaluated.

Acknowledgements

This work was supported by a grant from the Institute for Information & Communications Technology Promotion (IITP) funded by the Korean government (MSIT) (No. 2014-0-00282, Development of 5G Mobile Communication Technologies for Hyper-connected Smart Services).

References

- [1] K. Guan et al., "On Millimeter Wave and THz Mobile Radio Channel for Smart Rail Mobility," *IEEE Trans. Veh. Technol.*, vol. 66, no. 7, Nov. 2016, pp. 5658–5674.
- [2] B. Ai et al., "Future Railway Services-Oriented Mobile Communications Network," *IEEE Commun. Mag.*, vol. 53, no. 10, Oct. 2015, pp. 78–85.
- [3] X. Cheng et al., "An Improved Parameter Computation Method for a MIMO V2V Rayleigh Fading Channel Simulator under Non-isotropic Scattering Environments," *IEEE Commun. Lett.*, vol. 17, no. 2, Feb. 2013, pp. 265–268.
- [4] X. Cheng et al., "Communicating in the Real World: 3D MIMO," *IEEE Wirel. Commun.*, vol. 21, no. 4, Aug. 2014, pp. 136–144.
- [5] J. Zhang, Y. Zhang, Y. Yu, R. Xu, Q. Zheng, and P. Zhang, "3-D MIMO: How Much Does It Meet Our Expectations Observed from Channel Measurements?" *IEEE J. Sel. Areas Commun.*, vol. 35, no. 8, Aug. 2017, pp. 1887–1903.
- [6] X. Chen, "Experimental Investigation and Modeling of the Throughput of a 2×2 Closed-Loop MIMO System in a

- Reverberation Chamber,” *IEEE Trans. Antennas Propag.*, vol. 62, no. 9, Sept. 2014, pp. 4832–4835.
- [7] 5GCHAMPION project, Accessed Dec. 10, 2017. <http://www.5gchampion.eu>
- [8] J. Kim and I.G. Kim, “Distributed Antenna System-Based Millimeter Wave Mobile Broadband Communication System for High Speed Trains 2013,” *Int. Conf. ICT Convergence (ICTC)*, Jeju, Rep. of Korea, Oct. 14–26, 2013, pp. 218–222.
- [9] CMCC, “R1-163887 Update Evaluation Assumptions for NR High Speed Scenario,” 3rd Generation Partnership Project (3GPP) RAN1#84-BIS, Apr. 2016.
- [10] Mitsubishi Electric and ETRI, “R1-165484 WF on Evaluation Assumption for High Speed-Train Scenario 30 GHz,” 3rd Generation Partnership Project (3GPP) RAN1#85, May 2016.
- [11] Mitsubishi Electric, ETRI, and Ericsson, “R1-165926 WF on Additional Evaluation Assumptions for High Speed Train Scenario: Macro + Relay around 30 GHz,” 3rd Generation Partnership Project (3GPP) RAN1#85, May 2016.
- [12] X. Yin and X. Cheng, “Propagation Channel Characterization, Parameter Estimation, and Modeling for Wireless Communications,” Singapore: Wiley-IEEE Press, 2016.
- [13] M.K. Samimi and T.S. Rappaport, “3-D Millimeter-Wave Statistical Channel Model for 5G Wireless System Design,” *IEEE Trans. Microw. Theory Techn.*, vol. 64, no. 7, July 2016, pp. 2207–2225.
- [14] S. Hur et al., “Proposal on Millimeter-Wave Channel Modeling for 5G Cellular System,” *IEEE J. Sel. Topics Signal Process.*, vol. 10, no. 3, Apr. 2016, pp. 454–469.
- [15] W. Fan et al., “Measured Wideband Characteristics of Indoor Channels at Centimetric and Millimetric Bands,” *EURASIP J. Wirel. Commun. Netw.*, vol. 2016, no. 1, Feb. 2016, pp. 58:1–58:13.
- [16] J. Zhang et al., “6–100 GHz Research Progress and Challenges from a Channel Perspective for Fifth Generation (5G) and Future Wireless Communication,” *Sci. China Inform. Sci.*, vol. 60, no. 8, June 2017, p. 080301.
- [17] B. Ai et al., “Radio Wave Propagation Scene Partitioning for High-Speed Rails,” *Int. J. Antennas Propag.*, vol. 2012, no. 21, Oct. 2012, pp. 1072–1075.
- [18] J. Meinilä et al., “WINNER II channel models,” in *Radio Technologies and Concepts for IMT-Advanced*, Chichester, United Kingdom: John Wiley & Sons, 2008, pp. 39–92.
- [19] 3GPP, “Study on channel model for frequency spectrum above 6 GHz (Release 14),” TR 38.900 V14.3.1, July 2017.
- [20] S.W. Choi et al., “Performance Evaluation of Millimeter-Wave-Based Communication System in Tunnels,” *IEEE Globecom Workshops (GC Wkshps)*, San Diego, CA, USA, Dec. 6–10, 2015, pp. 1–5.
- [21] S. Priebe, M. Kannicht, M. Jacob, and T. Kürner, “Ultra Broadband Indoor Channel Measurements and Calibrated Ray Tracing Propagation Modeling at THz Frequencies,” *J. Commun. Netw.*, vol. 15, no. 6, Dec. 2013, pp. 547–558.
- [22] D. He et al., “Stochastic Channel Modeling for Kiosk Applications in the Terahertz Band,” *IEEE Trans. Terahertz Sci. Technol.*, vol. 7, no. 5, Sept. 2017, pp. 502–513.
- [23] V. Degli-Esposti, F. Fuschini, E.N. Vitucci, and G. Falciasecca, “Measurement and Modelling of Scattering from Buildings,” *IEEE Trans. Antennas Propag.*, vol. 55, no. 1, Jan. 2007, pp. 143–153.
- [24] 3GPP, “Spatial Channel Model for Multiple Input Multiple Output (MIMO) Simulations,” 3GPP TR 25.996, 2011, pp. 38–39.
- [25] S. Jaeckel, L. Raschke, K. Börner, and L. Thiele, “QuaDRiGa: A 3-D Multi-cell Channel Model with Time Evolution for Enabling Virtual Field Trials,” *IEEE Trans. Antennas Propag.*, vol. 62, no. 6, June 2014, pp. 3242–3256.



Danping He received her BS degree from Huazhong University of Science and Technology, Wuhan, China in 2008; her MS degree from the Université Catholique de Louvain, Belgium and Politecnico di Torino, Piemonte, Italy in 2010; and her PhD degree from Universidad Politécnica de Madrid, Spain in 2014. In 2012, she was a visiting scholar at the Institut national de recherche en informatique et en automatique, France. She worked at Huawei Technologies from 2014 to 2015 as a research engineer, and she is currently conducting postdoctoral research at the State Key Laboratory of Rail Traffic Control and Safety, Beijing Jiaotong University. Her current research interests include radio propagation and channel modeling, ray-tracing simulator development, and wireless communication algorithm design.



Bo Ai received his MS and PhD degrees from Xidian University, Xian, China in 2002 and 2004, respectively. He graduated with great honors as an Excellent Postdoctoral Research Fellow at Tsinghua University, Beijing, China in 2007. He is now working at Beijing Jiaotong

University, China, as a professor and advisor of PhD candidates. He is a deputy director of the State Key Lab of Rail Traffic Control and Safety. He is an associate editor for *IEEE Transactions on Consumer Electronics* and an editorial committee member of the journal *Wireless Personal Communications*. He has authored/coauthored 6 books, 140 scientific research papers, and 26 invention patents in his research area until now. His current interests are the research and applications of OFDM techniques, HPA linearization techniques, radio propagation and channel modeling, GSM for railway systems, and LTE for railway systems. He is an IET Fellow and IEEE Senior member.



Ke Guan received his BS degree and PhD degree from Beijing Jiaotong University, China in 2006 and 2014, respectively. He is an associate professor at the State Key Laboratory of Rail Traffic Control and Safety and the School of Electronic and Information

Engineering, Beijing Jiaotong University. In 2015, he was awarded a Humboldt Research Fellowship for Postdoctoral Researchers. He was the recipient of a 2014 International Union of Radio Science Young Scientist Award. He received six Best Paper Awards. In 2009, he was a visiting scholar at Universidad Politécnica de Madrid, Spain. From 2011 to 2013, he has been a research scholar at the Institut für Nachrichtentechnik at Technische Universität Braunschweig, Germany. From September 2013 to January 2014, he was invited to conduct joint research at Universidad Politécnica de Madrid, Spain. His current research interests are in the field of measurement and modeling of wireless propagation channels, high-speed railway communications, vehicle-to-x channel characterization, and indoor channel characterization for high-speed short-range systems including future terahertz communication systems.



Zhangdui Zhong is a professor and an advisor of PhD candidates at Beijing Jiaotong University, China. He is now a director of the School of Computer and Information Technology and a Chief Scientist at the State Key Laboratory of Rail Traffic Control and Safety in

Beijing Jiaotong University. He is also a director of the

Innovative Research Team of the Ministry of Education and a Chief Scientist of the Ministry of Railways in China. He is an executive council member of the Radio Association of China and a deputy director of the Radio Association of Beijing. His interests are wireless communications for railways, control theory and techniques for railways, and GSM-R system. His research has been widely used in railway engineering, such as the Qinghai-Xizang railway, the Datong-Qinhuangdao Heavy Haul railway, and many high-speed railway lines of China. He has authored/coauthored 7 books, 5 invention patents, and over 200 scientific research papers in his research area. He received the MaoYiSheng Scientific Award of China, the ZhanTianYou Railway Honorary Award of China, and the Top 10 Science/Technology Achievements Award of Chinese Universities.



Bing Hui received his BS degree in communication engineering from Northeastern University, Shenyang, China in 2005. He received his MS and PhD degrees at the Graduate School of Information Technology and Telecommunications, Inha University,

Incheon, Rep. of Korea 2009 and 2013, respectively. He was with the Electronic Engineering Department as a Postdoctoral Research Fellow from 2013 to 2014. Since 2014, he has been working as a researcher at the ETRI, Daejeon, Rep. of Korea. His research interests include the 3GPP LTE(-A)/5G systems, mmWave mobile wireless backhauling, MIMO techniques, optimal codebook design, and mobile Ad-Hoc networks.



Junhyeong Kim received his BS degree from the Department of Electronic Engineering at Tsinghua University, Beijing, China in 2008 and his MS degree from the Department of Electrical Engineering at the Korea Advanced Institute of Science and Technology

(KAIST), Daejeon, Rep. of Korea, in 2011. Since 2011, he has been with the ETRI, Daejeon, Rep. of Korea. He is also currently pursuing his PhD degree at the School of Electrical Engineering at KAIST. His main research interests include millimeter-wave communications, MIMO, and cooperative communications and handover.



Heesang Chung received his BS degree in physics from the Korea Advanced Institute of Science and Technology, Daejeon, Rep. of Korea in 1993 and his MS and PhD degrees from Chungnam National University, Daejeon, Rep. of Korea in 1995 and 1999, respectively.

Since then, he has been with the ETRI, Daejeon, Rep. of Korea, where he is currently a Principal Researcher. His career at ETRI began with optical communications, and he moved on to mobile and wireless communication systems in 2005. He was involved in research projects related to LTE and LTE-Advanced from 2006 to 2010. His recent research interests are in 5G with special emphasis on high-data-rate services for passengers on public transportation such as buses, subways, and bullet trains.



Ilgyu Kim received his BS and MS degrees in electronic engineering from the University of Seoul, Rep. of Korea in 1993 and 1995, and his PhD degree in information communications engineering from the Korea Advanced Institute of Science and Technology, Daejeon, Rep. of

Korea in 2009. Since 2000, he has been with the ETRI, Daejeon, Rep. of Korea, where he has been involved in the development of WCDMA, LTE, and MHN systems. Since 2012, he has been the leader of the mobile wireless backhaul research section. His main research interests include millimeter-wave communications and 5G mobile communications.